Structure and phonon density of states of supported size-selected ^{57}FeAu nanoclusters: A nuclear resonant inelastic x-ray scattering study

B. Roldan Cuenya,[1,a)] L. K. Ono,[1] J. R. Croy,[1] A. Naitabdi,[1] H. Heinrich,[1,2] J. Zhao,[3] E. E. Alp,[3] W. Sturhahn,[3] and W. Keune[4]
[1]*Department of Physics, University of Central Florida, Orlando, Florida 32816, USA*
[2]*Advanced Materials Processing and Analysis Center, University of Central Florida, Orlando, Florida 32816, USA*
[3]*Advanced Photon Source, Argonne National Laboratory, Argonne, Illinois 60439, USA*
[4]*Max-Planck-Institut für Mikrostrukturphysik, D-06120 Halle, Germany*

(Received 4 July 2009; accepted 2 September 2009; published online 5 October 2009)

We have measured the phonon density of states (PDOS) of isolated bcc and fcc Fe_xAu_{1-x} alloy nanoclusters (NCs) by nuclear resonant inelastic x-ray scattering. Drastic deviations were observed with respect to the PDOS of bulk Fe–Au alloys. Important information on the structure and thermodynamic properties of these NCs was obtained. © *2009 American Institute of Physics*. [doi:10.1063/1.3236539]

Metallic nanostructures are of great interest due to their intriguing size-dependent physical and chemical properties.[1] In the field of catalysis, oxide supported bimetallic nanoclusters (NCs) are known to exhibit remarkably high activities and enhanced selectivities.[2] Among the binary nanoscale alloys, Fe–Au constitutes an interesting material system for chemical, optical, magnetic, and biomedical applications.[3–6] Recently, we have investigated the thermal stability, segregation processes, and surface composition of Au–Fe NCs.[7] However, the atomic vibrational dynamics and the related thermodynamic properties are, so far, unexplored. Generally, dramatic differences between the vibrational (phonon) density of states (PDOS) $[g(E)]$ of bulk materials and isolated NCs have been reported.[8–10] Such modifications are of scientific and technological relevance because they profoundly affect the thermodynamic properties of the NCs. A detailed knowledge of the PDOS is the key for the understanding of lattice specific heat, vibrational entropy, and alloy phase stability.[11] We present an experimental study of the phonon spectrum of isolated, monodispersed, bcc and fcc ^{57}Fe–Au NCs via ^{57}Fe nuclear resonant inelastic x-ray scattering (NRIXS). Important thermodynamic properties of the NCs which are difficult to obtain by other methods are derived.

$^{57}Fe_xAu_{1-x}$ NCs with nominal compositions ($x=0.8, 0.5$) were synthesized by loading polystyrene-*b*-poly(2-vinylpyridine) micelles with $^{57}FeCl_3$ and $HAuCl_4$ salts.[7] $TiO_2(110)$ and $SiO_2/Si(111)$ substrates were dip-coated into the metal-loaded polymeric solutions and the organic ligands removed in ultrahigh vacuum (UHV) via an O_2-plasma treatment. The samples were then isochronally annealed in UHV at 300, 500, 700, and 850 °C for 30 min.

Figure 1 displays atomic force microscopy (AFM) images of our polymer-free $^{57}Fe_{0.8}Au_{0.2}$ NCs deposited on (a) $TiO_2(110)$ and (b) $SiO_2/Si(111)$, taken after annealing at 700 °C. The average cluster heights are 3.4 ± 1.0 and 1.8 ± 0.5 nm, respectively. The average height of the $^{57}Fe_{0.5}Au_{0.5}$ NCs at 700 °C was ~2.2 nm, and no significant changes in the cluster size or two-dimensional spatial arrangement were observed up to our maximum annealing temperature of 850 °C. High resolution transmission electron microscopy (TEM) images of $^{57}Fe_{0.5}Au_{0.5}$ NCs annealed at 700 and 900 °C are shown in Figs. 1(c) and 1(d), respectively. From the analysis of several TEM images acquired for each of these temperatures, average lattice parameters of 3.92(3) [Fig. 1(c)] and 3.91(3) Å [Fig. 1(d)] were obtained. These values are in good agreement with the lattice constant of bulk fcc $Fe_{47.5}Au_{52.5}$ alloys of 3.91 Å.[12]

X-ray photoelectron spectroscopy (XPS) can be used to investigate alloy formation (relative phase content) in Au–Fe NCs.[7] Figure 2 displays XPS (Fe 2*p*) spectra of $^{57}Fe_{0.5}Au_{0.5}$ [Figs. 2(a)–2(c)] and $^{57}Fe_{0.8}Au_{0.2}$ [Fig. 2(d)] NC samples supported on $TiO_2(110)$ and on $SiO_2/Si(111)$, respectively. The vertical reference lines indicate the binding energies of metallic Fe (Fe $2p_{3/2}$ at 707 eV), an Fe–Au alloy (711 eV), and of a smaller third component (Fe^*, 716.5 eV) assigned to the Fe-support interface (in the case of Au–Fe/TiO_2 the encapsulation of Fe by TiO_x is possible) and/or to satellite peaks of Fe (shake-up/shake-off).[7] After annealing at 500 °C, segregated Fe metal (~19%) coexists with the Fe–Au alloy (~47%) in the $^{57}Fe_{0.5}Au_{0.5}$ NCs. Further annealing at and above 700 °C results in an enhanced alloy content (52%–55%), with only ~5% and ~1% metallic Fe (Fe^0) present at 700 and 850 °C, respectively. A higher content of Fe^0 (~29%) is detected in the $^{57}Fe_{0.8}Au_{0.2}$ NCs after annealing at 700 °C versus ~35% Fe–Au alloy content.

NRIXS measurements were performed at room temperature (RT) in air at beamline 3-ID of the Advanced Photon Source (Argonne) by tuning the synchrotron beam energy around the resonant energy of 14.4125 keV of the ^{57}Fe nucleus with an energy resolution of ~1.2 meV. The NRIXS method and the data evaluation for extracting $g(E)$ are described in Refs. 13–16.

Figure 3 shows PDOS data extracted from NRIXS measurements on (a) $^{57}Fe_{0.8}Au_{0.2}$ and (b) $^{57}Fe_{0.5}Au_{0.5}$ NCs supported on $SiO_2/Si(111)$ and $TiO_2(110)$, respectively. The samples were annealed in UHV at the indicated temperatures. The Fe-projected PDOS of the Fe-rich $Fe_{0.8}Au_{0.2}$ NCs, Fig. 3(a), looks roughly similar to $g(E)$ of bulk bcc Fe with respect to the main peak positions. This proves the existence of a dominating Fe-rich bcc Fe–Au alloy in the NCs. This is in agreement with our XPS results and with the thermody-

a)Electronic mail: roldan@physics.ucf.edu.

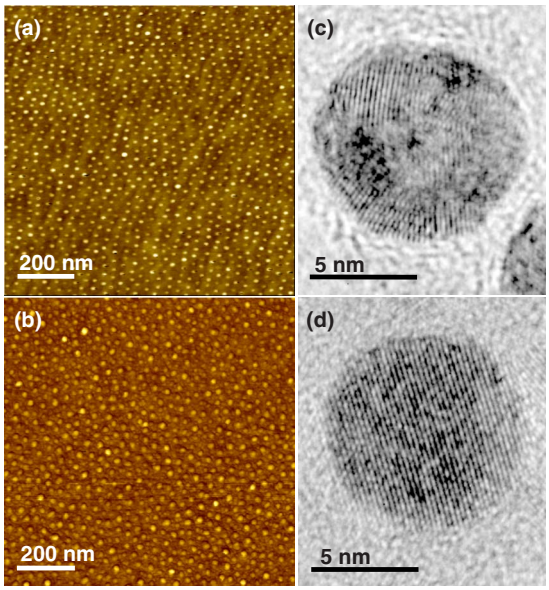

FIG. 1. (Color online) AFM images of $^{57}Fe_{0.8}Au_{0.2}$ NCs deposited on (a) $TiO_2(110)$ and (b) $SiO_2/Si(111)$, and TEM images of $^{57}Fe_{0.5}Au_{0.5}$ NCs on Ti-coated Ni grids. All images were taken after O_2-plasma treatment followed by annealing in UHV at [(a) and (c)] 700 and [(b) and (d)] 900 °C for 30 min. The TEM images were acquired on NCs synthesized with a polymer with larger head size PS(81000)-P2VP(14200), resulting in larger NCs than in the AFM/NRIXS samples.

namic phase diagram for bulk $Fe_{0.8}Au_{0.2}$ alloys at 700 °C.[17] The latter predicts phase separation into an Fe-rich majority phase of bcc $Fe_{0.99}Au_{0.01}$ (of ~67% phase content) and a Au-rich minority phase of fcc $Fe_{0.4}Au_{0.6}$ (~33% phase content). Despite the rough similarity of the two $g(E)$ curves in Fig. 3(a), the following deviations are observed: (i) a strong suppression of the longitudinal acoustic phonon peak of bcc Fe at ~36 meV that can be attributed to phonon confinement[10,18] and/or Au impurity atoms in the bcc phase.

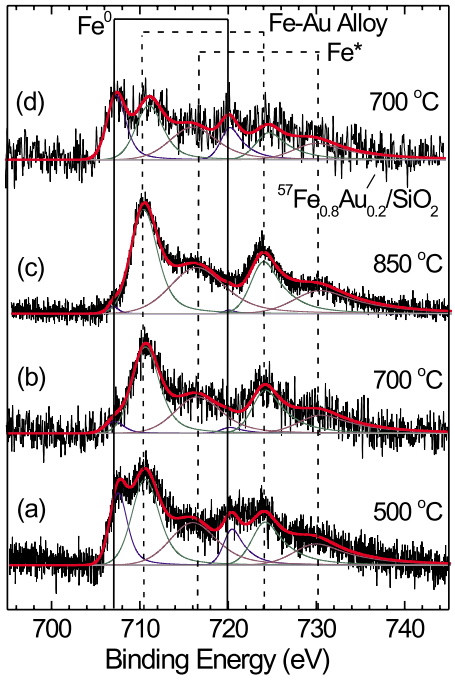

FIG. 2. (Color online) XPS (Fe 2*p*) spectra of [(a)–(c)] $^{57}Fe_{0.5}Au_{0.5}$ NCs supported on $TiO_2(110)$ and (d) $^{57}Fe_{0.8}Au_{0.2}$ NCs on $SiO_2/Si(111)$ acquired after O_2-plasma and annealing in UHV at the temperatures indicated.

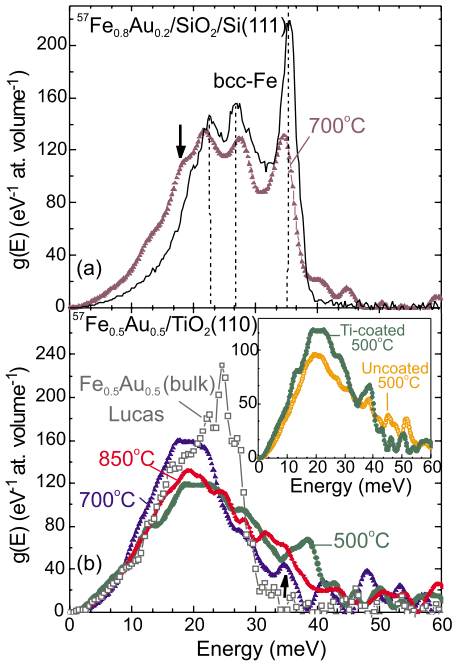

FIG. 3. (Color online) Fe-projected PDOS of (a) $^{57}Fe_{0.8}Au_{0.2}$ NCs on $SiO_2/Si(111)$ and (b) $^{57}Fe_{0.5}Au_{0.5}$ NCs on $TiO_2(110)$ after O_2-plasma treatment and annealing in UHV at (b) 500, [(a) and (b)] 700, and (b) 850 °C for 30 min. The NCs in (a) are uncoated and in (b) are protected by a 5 nm Ti layer. For reference, $g(E)$ of bulk bcc Fe is shown in (a) and of a bulk $Fe_{0.5}Au_{0.5}$ alloy from Ref. 20 in (b). The inset in (b) displays $g(E)$ of uncoated and Ti-coated $^{57}Fe_{50}Au_{50}$ NCs annealed at 500 °C.

These effects might also lead to the small redshift observed (~1 meV) for the main $g(E)$ peaks of the $Fe_{0.8}Au_{0.2}$ NCs. (ii) A pronounced enhancement and shift in the low-E part (at $E < \sim 20$ meV) of the NCs' PDOS toward lower phonon energies, combined with the appearance of a shoulder near ~18 meV [arrow in Fig. 3(a)]. Based on our XPS results, and on the Fe–Au phase diagram, the latter effects are attributed to the contribution of the Au-rich minority fcc $Fe_{0.4}Au_{0.6}$ phase. (iii) A weak $g(E)$ contribution near ~40–44 meV, i.e., above the cutoff energy of bcc Fe. This contribution might be related to the presence of a small fraction of Fe oxides on the NC surface or at the NC/support interface.

After annealing in UHV, the $^{57}Fe_{0.5}Au_{0.5}$ NCs were coated (at RT) by a protective film of 5 nm Ti. The PDOS of these NCs annealed at 500 °C [Fig. 3(b)] reveals a peak at ~38 meV characteristic of segregated bcc-Fe grains. This peak position is slightly higher than that of bulk bcc-Fe (~36 meV). This could be due to intrinsic capillary pressure[19] or to compressive strain in the bcc nanograins. Most importantly, the broad peak detected around ~19–21 meV in Fig. 3(b) (for 500 °C) signalizes the formation of a Au-rich fcc Fe–Au alloy, in addition to the bcc Fe alloy phase (see below). These results are in agreement with the XPS data shown above. The inset in Fig. 3(b) demonstrates that Ti coating of the $Fe_{0.5}Au_{0.5}$ NCs results in an enhancement in the broad band near ~20 meV at expense of the $g(E)$ contribution above ~42 meV (generally attributed to Fe oxides)[10] without significantly affecting the overall shape of $g(E)$ below ~40 meV. Further annealing at 700 °C results in sharpening and in a remarkable increase in the $g(E)$ peak near ~19 meV (Au-rich fcc alloy), accompanied by a decrease in the height and a redshift to ~35 meV of the

TABLE I. Thermodynamic parameters at 295 K: Lamb–Mössbauer factor (f_{LM}), Debye temperature (θ_D), kinetic energy (E_k), vibrational entropy (S_{vib}), and vibrational specific heat at constant volume (C_{vib}).

Sample	f_{LM}	θ_D (K)	E_k (meV/atom)	S_{vib} (k_B/atom)	C_{vib} (k_B/atom)
$Fe_{0.8}Au_{0.2}$NCs/Si	0.722	381.9	42.6	3.33	2.73
700 °C, uncoated	(3)	(3)	(3)	(3)	(4)
$Fe_{0.5}Au_{0.5}$NCs/TiO_2	0.689	388.6	44.4	3.11	2.61
500 °C, uncoated	(2)	(3)	(3)	(3)	(4)
$Fe_{0.5}Au_{0.5}$NCs/TiO_2	0.599	331.0	41.7	3.63	2.77
500 °C, Ti-coated	(3)	(4)	(6)	(5)	(6)
$Fe_{0.5}Au_{0.5}$NCs/TiO_2	0.657	320.6	41.1	3.82	2.81
700 °C, Ti-coated	(3)	(4)	(7)	(5)	(7)
$Fe_{0.5}Au_{0.5}$NCs/TiO_2	0.658	345.8	42.2	3.56	2.75
850 °C, Ti-coated	(3)	(4)	(5)	(4)	(6)
Fe NCs (bcc)/Si	0.611	384.3	45.0	2.95	2.6
500 °C, Si-coated (Ref. 10)	(3)	(8)	(9)	(7)	(1)
Bulk bcc-Fe	0.7951	423.74	42.54	3.133	2.723
	(6)	(9)	(6)	(9)	(9)

bcc-Fe alloy peak [arrow in Fig. 3(b)]. These features indicate the formation of a majority Au-rich fcc Fe–Au alloy phase with a small amount of Fe-rich bcc Fe–Au alloy. This agrees with our XPS findings and with the bulk phase diagram at $x=0.5$ and 700 °C, which predicts phase separation into a dominant Au-rich fcc $Fe_{0.4}Au_{0.6}$ alloy (of ~83% phase content) and an Fe-rich minority phase of bcc $Fe_{0.99}Au_{0.01}$ (of only ~17% phase content). At 850 °C, the bulk phase diagram discloses a stable $Fe_{0.5}Au_{0.5}$ alloy without segregation (single phase). In fact, our PDOS of $Fe_{0.5}Au_{0.5}$ NCs (at 850 °C) also indicates the formation of a Au-rich fcc Fe–Au alloy (majority phase) via the broad $g(E)$ peak centered at ~19 meV [Fig. 3(b)]. However, a reduced ~19 meV height (fcc alloy), as well as asymmetric broadening and $g(E)$ enhancement at higher energies, is observed at 850 °C as compared to the case of 700 °C. According to our XPS data, only a minimum amount (~1%) of metallic Fe is present at 850 °C. Therefore, the observed peak broadening might be attributed to a change in chemical short range order (Fe cluster formation) in the fcc $Fe_{0.4}Au_{0.6}$ alloy at 850 °C, leading to an increased number of Fe–Fe neighboring atoms with stronger Fe–Fe force constants and, consequently, to $g(E)$ enhancement at higher phonon energies.

A comparison of the PDOS of our $^{57}Fe_{0.5}Au_{0.5}$ NCs to that of bulk $^{57}Fe_{0.5}Au_{0.5}$ alloys from Lucas[20] reveals two main differences: (i) a strong suppression of bulk phonon modes between ~20–30 meV in the NCs, possibly due to phonon confinement,[18] and (ii) an increase in $g(E)$ above ~30 meV in the NCs. The latter effect can originate either from segregated bcc-Fe alloy grains in the NCs (annealed at 500 °C and 700 °C) and/or from Fe cluster formation in the fcc alloy of the NCs (at 850 °C). One can also notice that all $g(E)$ curves shown in Fig. 3(b) merge below ~10 meV.

Several thermodynamic quantities were obtained from our PDOS, Table I. The Lamb–Mössbauer factor and the Debye temperature of all of our ^{57}Fe–Au and ^{57}Fe NCs are smaller than those of bulk bcc Fe. The kinetic energy of the NCs is similar to that of bulk bcc Fe, but higher values were found on the NCs where Fe oxide species might be present [uncoated $^{57}Fe_{0.5}Au_{0.5}$ (500 °C) sample and pure ^{57}Fe NCs (Ref. 10)]. The vibrational entropy of our NCs is similar to that of bulk bcc Fe, while larger values were obtained for the Ti-coated $^{57}Fe_{0.5}Au_{0.5}$ NCs, where a Au-rich fcc alloy was formed. The vibrational specific heat of our NC samples is also similar to that of bulk bcc Fe, with only a small decrease observed on the two samples containing oxidized Fe species mentioned above.

In summary, we have shown that NRIXS is capable of following segregation trends in systems comprised of isolated, supported, bimetallic Fe–Au NCs. In addition, important thermodynamic properties of these systems may be derived. The applicability of this type of study to other NRIXS-relevant bimetallic systems is supposed.[21]

Funding from NSF (Grant Nos. CAREER-DMR-0448491 and DMR-0906562) and U.S. DOE (Grant No. DE-AC02-06CH11357) is greatly appreciated.

[1] H. J. Freund, Surf. Sci. **500**, 271 (2002).
[2] A. M. Molenbroek, J. K. Norskov, and B. S. Clausen, J. Phys. Chem. B **105**, 5450 (2001).
[3] R. M. Finch, N. A. Hodge, G. J. Hutchings, A. Meagher, Q. A. Pankhurst, M. R. H. Siddiqui, F. E. Wagner, and R. Whyman, Phys. Chem. Chem. Phys. **1**, 485 (1999).
[4] Q. Sun, A. K. Kandalam, Q. Wang, P. Jena, Y. Kawazoe, and M. Marquez, Phys. Rev. B **73**, 134409 (2006).
[5] Y. P. Lee, Y. V. Kudryavtsev, V. V. Nemoshkalenko, R. Gontarz, and J. Y. Rhee, Phys. Rev. B **67**, 104424 (2003).
[6] K. Takanashi, S. Mitani, K. Himi, and H. Fujimori, Appl. Phys. Lett. **72**, 737 (1998).
[7] A. Naitabdi, L. K. Ono, F. Behafarid, and B. Roldan Cuenya, J. Phys. Chem. C **113**, 1433 (2009).
[8] A. Kara and T. Rahman, Surf. Sci. Rep. **56**, 159 (2005).
[9] S. R. Calvo and P. B. Balbuena, Surf. Sci. **581**, 213 (2005).
[10] B. Roldan Cuenya, A. Naitabdi, J. Croy, W. Sturhahn, J. Y. Zhao, E. E. Alp, R. Meyer, D. Sudfeld, E. Schuster, and W. Keune, Phys. Rev. B **76**, 195422 (2007).
[11] B. Fultz, "Vibrational thermodynamics of materials," Prog. Mater. Sci. (to be published).
[12] W. B. Pearson, *A Handbook of Lattice Spacings and Structures of Metals and Alloys* (Pergamon, Oxford, 1964), Vol. 1.
[13] M. Seto, Y. Yoda, S. Kikuta, X. W. Zhang, and M. Ando, Phys. Rev. Lett. **74**, 3828 (1995).
[14] W. Sturhahn, T. S. Toellner, E. E. Alp, X. Zhang, M. Ando, Y. Yoda, S. Kikuta, M. Seto, C. W. Kimball, and B. Dabrowski, Phys. Rev. Lett. **74**, 3832 (1995).
[15] A. I. Chumakov, R. Ruffer, H. Grunsteudel, H. F. Grunsteudel, G. Grubel, J. Metge, and H. A. Goodwin, Europhys. Lett. **30**, 427 (1995).
[16] W. Sturhahn, Hyperfine Interact. **125**, 149 (2000).
[17] M. Hansen and K. Anderko, *Constitution of Binary Alloys* (McGraw-Hill, New York, 1958).
[18] B. Roldan Cuenya, W. Keune, R. Peters, E. Schuster, B. Sahoo, U. von Hörsten, W. Sturhahn, J. Zhao, T. S. Toellner, E. E. Alp, and S. D. Bader, Phys. Rev. B **77**, 165410 (2008).
[19] M. S. Lucas, Thesis, California Institute of Technology, 2008.
[20] R. Meyer, S. Prakash, and P. Entel, Phase Transitions **75**, 51 (2002).
[21] B. Roldan Cuenya, J. R. Croy, L. K. Ono, A. Naitabdi, H. Heinrich, W. Keune, J. Zhao, W. Sturhahn, E. E. Alp, and M. Hu, Phys. Rev. B **80**, 125412 (2009).